

Electronic Supplementary Information (ESI)

**Metal-organic framework derived Co,N-bidoped carbons as superior electrode
catalysts for quantum dot sensitized solar cells**

**Yan Li,^{*a} Leilei Zhao,^a Zhonglin Du,^a Jun Du,^a Wei Wang,^a Yuan Wang,^a Lianjing Zhao,^a Xiao-Ming
Cao,^{*b} and Xinhua Zhong^c**

^aShanghai Key Laboratory of Functional Materials Chemistry , Key Laboratory for Advanced Materials, School of Chemistry and Molecular Engineering, East China University of Science and Technology, Shanghai 200237, China

^bKey Laboratory for Advanced Materials, Center for Computational Chemistry and Research, Institute of Industrial Catalysis, East China University of Science and Technology, Shanghai 200237, China

^cCollege of Materials and Energy, South China Agricultural University, Guangzhou 510642, China

*Email: yli@ecust.edu.cn (for Y. L.); xmcao@ecust.edu.cn (for X.-M. C)

Fax: (+86) 21 6425 0281

Table of contents

- 1. Experimental Section.**
- 2. Characterization.**
- 3. Supporting Figures and Tables.**
- 4. Density Function Theory Calculation Details.**
- 5. References**

1. Experimental Section

Chemicals.

Oleylamine (OAm, 95%), selenium powder (200 mesh, 99.99%), 1-octadecene (ODE, 90%) were purchased from Aldrich. Diphenylphosphine (DPP, 98%), zinc acetate ($\text{Zn}(\text{OAc})_2 \cdot 2\text{H}_2\text{O}$, 99.99%) and 2-methylimidazole (99%) was obtained from ACROS Organics. Indium acetate ($\text{In}(\text{OAc})_3$, 99.99%), copper iodide (CuI , 99.998%), and 3-mercaptopropionic acid (MPA, 98%) were received from Alfa Aesar. Cobalt Nitrate Hexahydrate ($\text{Co}(\text{NO}_3)_2 \cdot 6\text{H}_2\text{O}$ 99%), poly(vinylpyrrolidone) (PVP, $M_w = 8000$) and ethyl cellulose were purchased from Sinopharm Chemical Reagent Co.,Ltd. Zinc nitratehexahydrate ($\text{Zn}(\text{NO}_3)_2 \cdot 6\text{H}_2\text{O}$, 99%), methanol (AR) and sulfuric acid (H_2SO_4 , 98%), melamine (CP) and formaldehyde (37%–40%) were purchased from Shanghai Ling Feng Chemical Reagent Co., Terephthalic acid Ltd. were purchased from Tokyo Chemical Industry Co., Ltd. All reagents were used without any further treatment.

Synthesis of water-soluble Zn-Cu-In-Se QDs.

Following the reported method, the oil-soluble Zn-Cu-In-Se QDs were synthesized *via* a facile hot-injection approach.¹ First, Zn stock solution was obtained by dissolving $\text{Zn}(\text{OAc})_2 \cdot 2\text{H}_2\text{O}$ (110 mg, 0.5 mmol) into a mixture of 0.5 mL OAm and 4.5 mL ODE at 120 °C and Se stock prepared by dissolving Se powder (24 mg, 0.3 mmol) into a mixture of 0.3 mL DPP and 0.5 mL OAm. Then, CuI (19.0 mg, 0.1 mmol), $\text{In}(\text{OAc})_3$ (29.0 mg, 0.1 mmol), OAm (2.0 mL), ODE (1.5 mL) and 0.4 mL of the obtained Zn stock solution were loaded in a 50 mL three necked flask and heated to 200 °C under N_2 atmosphere. Subsequently, the prepared Se precursor was quickly injected into the above reaction system. After reacting for 5 min, the system was cooled to 90 °C, and the OAm-capped Zn-Cu-In-Se QDs were obtained. The crude oil-soluble Zn-Cu-In-Se QDs were purified by centrifugation and decantation with a balanced amount of ethanol and acetone.

The oil-soluble Zn-Cu-In-Se QDs were further transferred into water-soluble *via* ligand exchange method.² Generally, 1.0 mL of MPA-methanol solution (2.0 mmol of MPA was added in 1.0 mL of methanol, and the pH value was adjusted to 10.0 using 30% NaOH aqueous solution) was added into the prepared oil-soluble Zn-Cu-In-Se QDs solution. After stirring for 2 min, the MPA capped Zn-Cu-In-Se QDs were extracted from CH_2Cl_2 into water phase by adding deionized water under vigorously stirring. The obtained MPA capped Zn-Cu-In-Se QDs were purified by centrifugation and decantation

with acetone, and redispersed in 1.0 mL deionized water. The pH value of the QD dispersion was finally adjusted to 10.0 with 10% NaOH aqueous solution.

Synthesis of Mesoporous Carbon (MC) and N-doped MC (N-MC) from organics.

According to the reported method,³ the MC was prepared by a colloidal silica assisted sol-gel procedure using formaldehyde and phenol as precursors. Typically, the mixture of 9.41 g (37 wt%, 116 mmol) of formaldehyde solution, 5.51 g (58 mmol) of phenol and 35 mL of 0.2 M NaOH solution was stirred at 70 °C for 40 min followed by the addition of 50 g of Ludox SM-30 sol (30 wt% SiO₂). After diluting to 100 mL with water, the resultant solution was transferred to a sealed bottle and heated at 80 °C for 3 days to give a gel. After drying at 80 °C in an ambient condition, the gel was carbonized at 800 °C for 3 h under N₂ atmosphere followed by alkali washing (2.0 M NaOH solution at 80 °C for 12 h) and acid washing (2 M hydrochloric acid at 60 °C for 5 h). The obtained powders were then washed using HF solution (2.0 M) and distilled water, and finally dried at 100 °C. With the similar procedure to the above MC, N-doped MC were prepared following a literature method, during which melamine with the mole ratio of melamine/phenol of 2 was used to offer N atom doping.⁴

2. Characterization.

Materials Characterization.

The morphology characterization of the samples was analyzed by scanning electron microscopy (SEM, NOVANano, FET) and transmission electron microscopy (TEM, JEM-2100, JEOL). X-ray diffraction (XRD) test was conducted using an automatic D5005 X-ray powder diffractometer from Siemens. Raman shift was measured using an inVia Reflex Raman microspectrometer from Renishaw. Brumauer-Emmett-Teller surface areas (S_{BET}) were measured with an ASAP2010N machine from Macromeritics. An ESCALAB 250 equipment of Thermo-VG Scientific was used for the X-ray photoelectron spectroscopy (XPS) measurements.

Photovoltaic performance Characterization.

J - V curves were obtained by a solar simulator (AM 1.5, Oriel, model no. 91160, Keithley 2400 source meter) equipped with a 150 W xenon lamp. The luminous intensity was calibrated to 100 mW·cm⁻² with use of a NREL standard Si solar cell. The photoactive area of QDSCs is 0.236 cm². Electrochemical impedance spectroscopy (EIS), Tafel polarization spectroscopy measurements were performed in dark condition with use of a sandwich type dummy cell composed of two face to face

identical CEs. The measurements were conducted by a CIMPS-2 system equipped Zennium workstation (Zahner, Germany). The EIS measurements were conducted on a scan frequency from 100 mHz to 100 kHz with an amplitude of 10 mV. Tafel polarization spectroscopy measurements were received on a scan frequency of 50 mV/s with the edge potential from -800 mV to 800 mV, and the current range from -2.5 A to 2.5 A. Cyclic voltammetry (CV) measurements were gained by the same apparatus as EIS and Tafel polarization spectroscopy measurements with a three-electrode system (platinum wire served as an auxiliary electrode, standard calomel electrode acted as a reference electrode, and the studied CE is working electrode). The active area of the studied CEs is 0.36 cm² and the electrolyte employed is a modified polysulfide electrolyte water solution modified (consists 2.0 M Na₂S and 2.0 M S, 0.2 M KCl and 20 wt% PVP).

2. Supporting Figures and Tables.

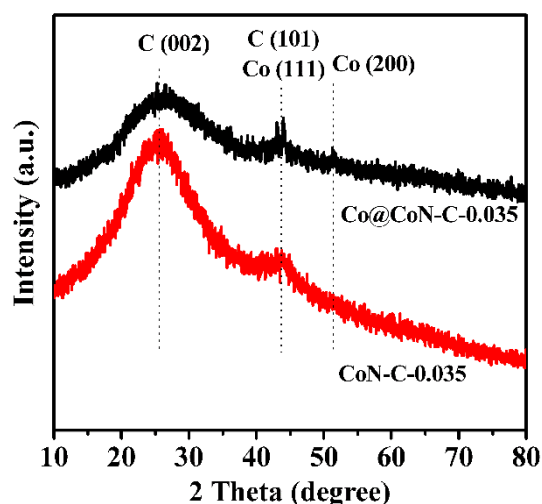


Fig. S1. Powder XRD patterns corresponding for Co@CoN-C-0.035 and CoN-C-0.035.

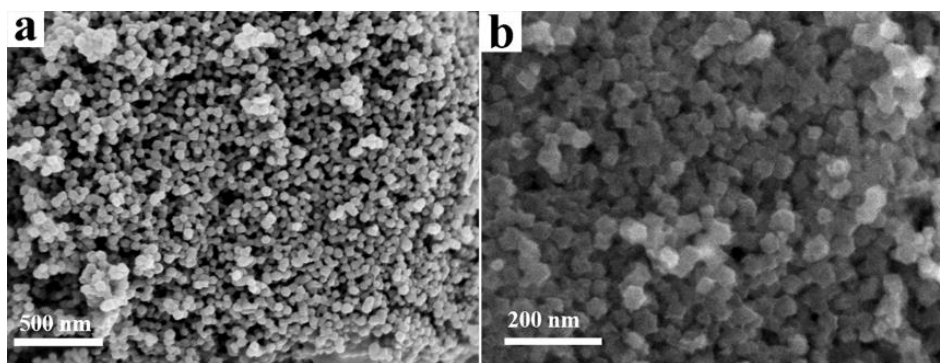


Fig. S2. SEM image of (a) ZIF-0.035, (b) CoN-C-0.035 samples.

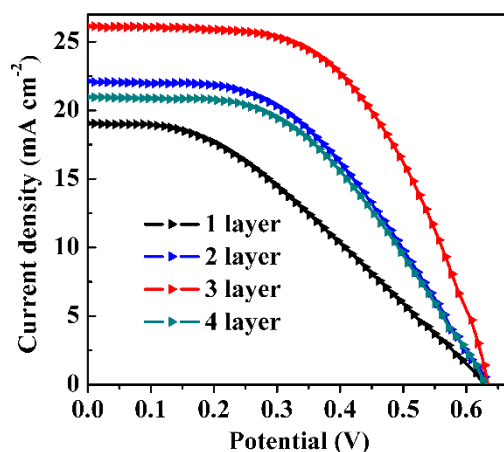


Fig. S3. J - V curves of Zn-Cu-In-Se QDSCs based on CoN-C-0.035 CEs with different layers.

The effect of the thickness of carbon film layers in CE on the photovoltaic performance of QDSC devices was surveyed first during which CoN-C-0.035 was used as the representative of carbons. With the increase in carbon film thickness from 1 to 3 layer, open-circuit voltage (V_{oc}) almost remains unchanged, but short circuit current density (J_{sc}) and fill factor (FF) are improved systematically, as illustrated in Fig. S3 and Table S1. A further increase in the catalyst thickness (from 3 to 4 layers) however leads to an obvious decline of PCE from 9.05 to 6.29%. Although a thicker carbon film contains more active sites favorable for polysulfide reduction, it goes against the electron transport and electrolyte diffusion in the CEs. Furthermore, the films are tend to be fractured and peel off from the FTO glass, which is unfavorable for the long-term stability of the cell devices constructed.

Table S1. Individual and average photovoltaic parameter values of Zn-Cu-In-Se QDSCs based on CoN-C-0.035 CEs with different layers under standard conditions (AM 1.5 G, 100 mW/cm²).

Layer	V_{oc} (V)	J_{sc} (mA·cm ⁻²)	FF	PCE (%)
1	0.625	19.02	0.368	4.37
	0.620	19.22	0.365	4.35
	0.624	19.20	0.358	4.29
	0.627	19.30	0.355	4.25
	0.623	19.17	0.360	4.30
Average	0.624±0.003	19.18±0.10	0.361±0.005	4.31±0.05
2	0.635	22.10	0.467	6.55
	0.630	22.20	0.465	6.45
	0.632	22.35	0.460	6.50
	0.622	22.15	0.470	6.48
	0.631	22.25	0.462	6.49

	0.625	22.16	0.472	6.54
Average	0.629±0.005	22.19±0.095	0.467±0.005	6.50±0.041
	0.635	26.15	0.549	9.12
	0.633	26.04	0.552	9.10
3	0.630	25.99	0.550	9.05
	0.636	26.26	0.540	9.02
	0.629	26.11	0.545	8.95
Average	0.633±0.003	26.11±0.10	0.547±0.005	9.05±0.07
	0.636	20.97	0.475	6.38
	0.635	20.80	0.474	6.25
4	0.628	21.14	0.475	6.30
	0.644	20.99	0.460	6.22
	0.630	20.99	0.475	6.28
Average	0.635±0.006	20.98±0.12	0.472±0.007	6.29±0.06

Table S2. Individual and average photovoltaic parameter values of Zn-Cu-In-Se QDSCs based on different CEs under standard conditions (AM 1.5 G, 100 mW/cm²).

CEs	V_{oc} (V)	J_{sc} (mA·cm ⁻²)	FF	PCE (%)
	0.638	22.81	0.501	7.30
	0.642	23.04	0.490	7.25
CoN-C-0	0.645	22.66	0.489	7.15
	0.635	22.86	0.498	7.23
	0.634	22.95	0.495	7.20
Average	0.639±0.005	22.86±0.14	0.495±0.005	7.23±0.06
	0.637	25.16	0.534	8.56
	0.633	24.81	0.540	8.48
CoN-C-0.025	0.630	25.12	0.537	8.50
	0.632	24.96	0.538	8.49
	0.629	25.31	0.530	8.44
Average	0.632±0.003	25.07±0.19	0.536±0.004	8.49±0.04
	0.635	26.15	0.549	9.12
	0.633	26.04	0.552	9.10
CoN-C-0.035	0.633	25.99	0.550	9.05
	0.636	26.26	0.540	9.02

	0.629	26.11	0.545	8.95
Average	0.633±0.003	26.11±0.10	0.547±0.005	9.05±0.07
	0.630	25.99	0.541	8.86
	0.635	25.76	0.538	8.80
CoN-C-0.05	0.625	25.78	0.543	8.75
	0.627	26.06	0.530	8.66
	0.630	25.74	0.545	8.84
Average	0.629±0.004	25.87±0.15	0.539±0.006	8.78±0.08
	0.628	24.22	0.539	8.20
	0.625	24.60	0.530	8.15
CoN-C-0.1	0.620	24.47	0.534	8.10
	0.622	24.58	0.535	8.18
	0.627	24.51	0.529	8.13
Average	0.624±0.003	24.48±0.15	0.533±0.004	8.15±0.04
	0.621	23.90	0.532	7.89
	0.617	23.83	0.529	7.78
	0.622	23.80	0.532	7.88
CoN-C-1	0.615	23.79	0.530	7.75
	0.619	23.68	0.532	7.80
Average	0.619±0.003	23.80±0.08	0.531±0.001	7.82±0.06
	0.637	23.70	0.425	6.42
	0.635	23.67	0.425	6.39
C-MOF-5	0.637	23.55	0.420	6.30
	0.644	23.75	0.415	6.35
	0.649	23.60	0.418	6.40
Average	0.640±0.006	23.65±0.08	0.421±0.004	6.37±0.05
	0.630	24.22	0.400	6.10
	0.637	24.15	0.390	6.00
N-MC	0.635	24.12	0.395	6.05
	0.635	24.13	0.385	5.90
	0.630	24.00	0.402	6.08
Average	0.633±0.003	24.12±0.08	0.394±0.007	6.03±0.08
	0.638	24.17	0.361	5.57
	0.637	24.11	0.361	5.54
MC	0.636	23.95	0.358	5.45

	0.640	24.01	0.350	5.38
	0.640	23.88	0.360	5.50
Average	0.638±0.002	24.02±0.12	0.358±0.005	5.49±0.08
	0.630	24.45	0.458	7.05
	0.627	24.35	0.457	6.98
AC	0.634	24.28	0.448	6.90
	0.627	24.40	0.450	6.88
	0.625	24.07	0.452	6.80
Average	0.629±0.004	24.31±0.148	0.453±0.004	6.92±0.10

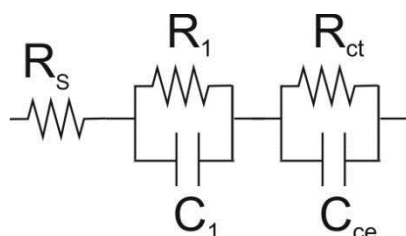


Fig. S4. Simulation circuit used for analyzing the EIS data for symmetric dummy cells. R_s accounts for substrate resistance, R_1 and C_1 associated to high frequency arc, for charge transfer resistance and contact capacitance at interface between substrate and carbon electrode, R_{ct} and C_{ce} associated to low frequency arc, for charge transfer resistance and electrode capacitance at CE/electrolyte interface.

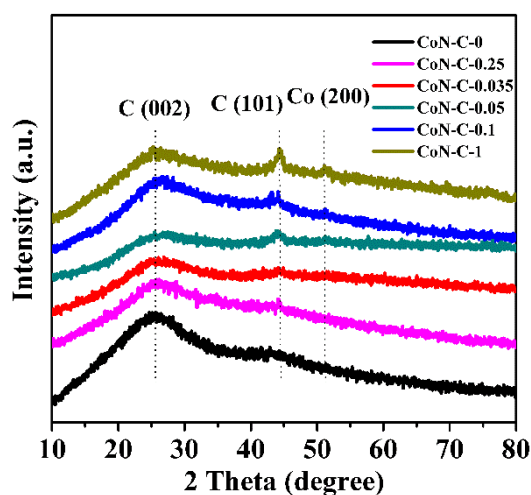


Fig. S5. The power XRD patterns for CoN-C- n samples.

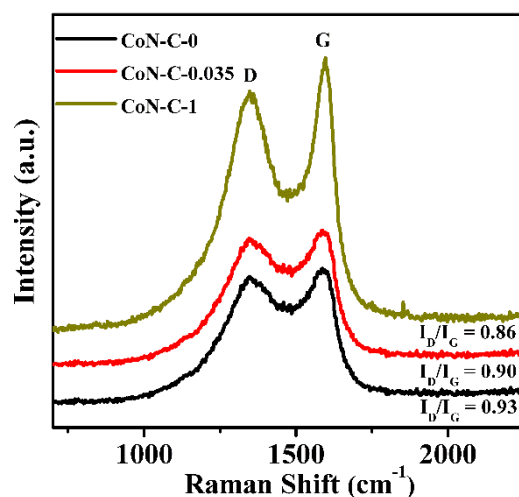


Fig. S6. Raman spectra for CoN-C-0, CoN-C-0.035 and CoN-C-1 samples.

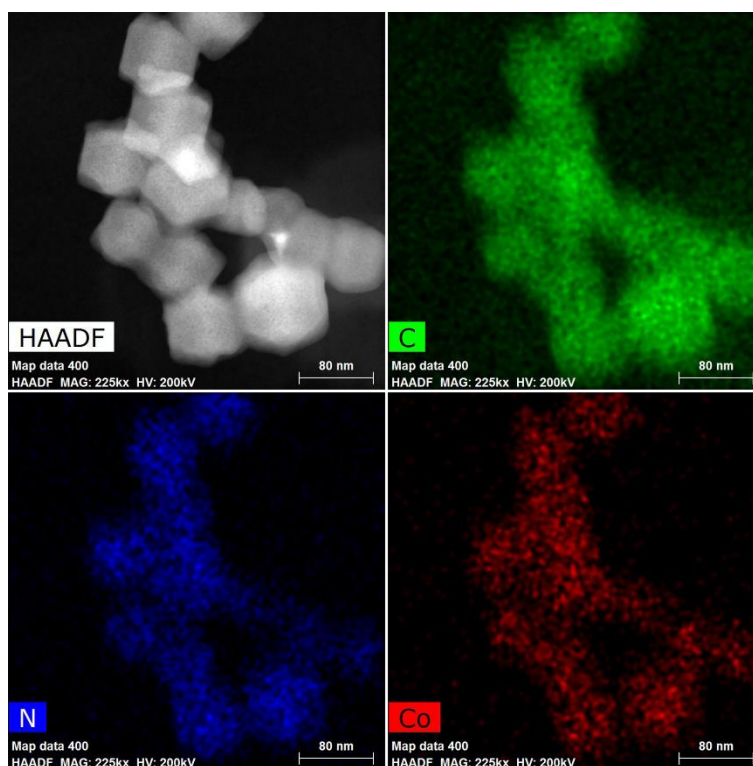


Fig. S7. Dark field STEM image of CoN-C-0.035 and the corresponding elemental mapping for C, N, and Co.

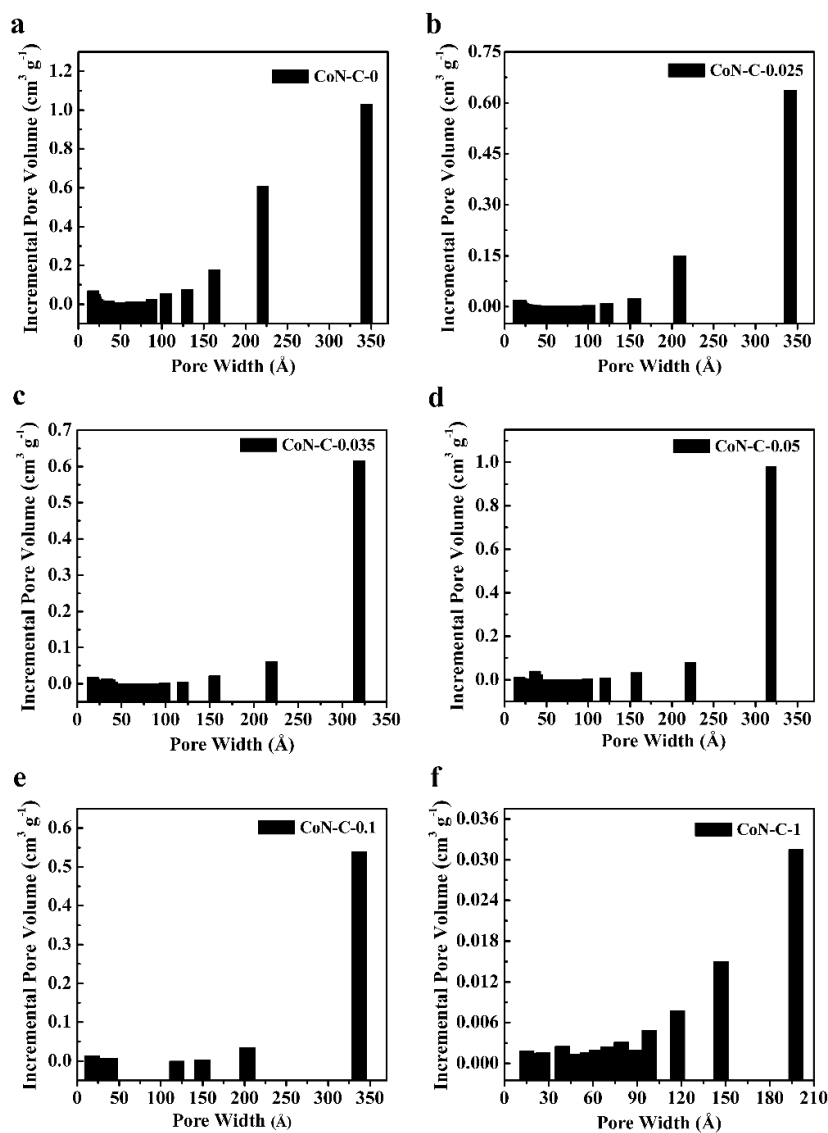
Table S3. N 1s analysis of XPS spectra in CoN-C-0.035 sample.

N-type	graphitic-N	pyrrolic-N	pyridinic-N	Co-N _x	oxidized-N
Binding Energy (eV)	401.4	400.5	398.5	399.2	404.1
Area (%)	25.25	17.21	24.53	27.50	5.51

Table S4. Pore parameters of CoN-C-*n* and C-MOF-5 samples.

Sample	CoN-C-0	CoN-C-0.025	CoN-C-0.035	CoN-C-0.05	CoN-C-0.1	CoN-C-1	C-MOF-5
$S_{\text{BET}}^a (\text{m}^2 \text{g}^{-1})$	1818	1200	1081	893	681	206	1919
$V_{\text{total}}^b (\text{cm}^3 \text{g}^{-1})$	1.92	0.770	0.745	0.731	0.448	0.171	2.05

^a BET specific surface area; ^b Total pore volume ($p/p_0=0.950$).

**Fig. S8.** Pore size distributions for CoN-C-*n* samples calculated by BJH desorption method.

4. Density Function Theory Calculation Details.

All the free energies of the reactions in the aqueous solution and the standard reduction potentials were modeled utilizing hybrid meta-gga M06-2x functional⁵ with the triple- ζ basis set def2-TZVPP⁶ implemented in Gaussian 09 suite. The hydration free energies of polysulfide were simulated

combining both explicit and implicit model. The geometry structures of neutral, monoanionic and dianionic polysulfide cluster with 0, 1, 2 and 4 explicit water models were respectively optimized with the introduction of integral equation formalism version of Polarizable continuum model (IEF-PCM)⁷ as well. The free energies of the reactions ΔG_∞ were obtained *via* extrapolating the free energies against the number of water molecules n to ∞ based on the form of $\Delta G_n = \Delta G_\infty + ae^{-bn}$. 4.44 V is chosen as the absolute potential of RHE.⁸

To obtain the free adsorption energy of S_2^- , $G_{ad}^{S_2^-}$, the spin polarized periodic DFT calculations were carried out to simulate the adsorption and desorption process utilizing Perdew-Burke-Ernzerhof (PBE) functional⁹ with the Grimme's empirical three-body dispersion correction in the scheme of Becke-Johnson damping¹⁰ implemented in VASP package¹¹. The electron-ion interactions were modeled utilizing the projector augmented wave (PAW) pseudopotential and the plane wave basis-set was expanded to the converged cut-off energy of 500 eV. The pristine graphene was modeled utilizing a p (4×2) slab with the size of $9.874 \text{ \AA} \times 8.551 \text{ \AA} \times 20.000 \text{ \AA}$. The N-graphene was modeled by doping two N at the para position of one benzene ring at graphene.¹² The Co-N₄@graphene was adopted to model Co,N-bidoped carbon materials which has been observed by Bao et al.¹³ The corresponding Brillouin integration for the unit cell was sampled using $2 \times 3 \times 1$ Monkhorst-Pack grid. Three layers of water molecules with sodium ion were explicitly introduced into the solid-liquid interface for the solvation effect. $G_{ad}^{S_2^-}$ are defined as follows:

$$G_{ad}^{S_2^-} = G_{S_2^-(aq)} - G_{S_2^-*}$$

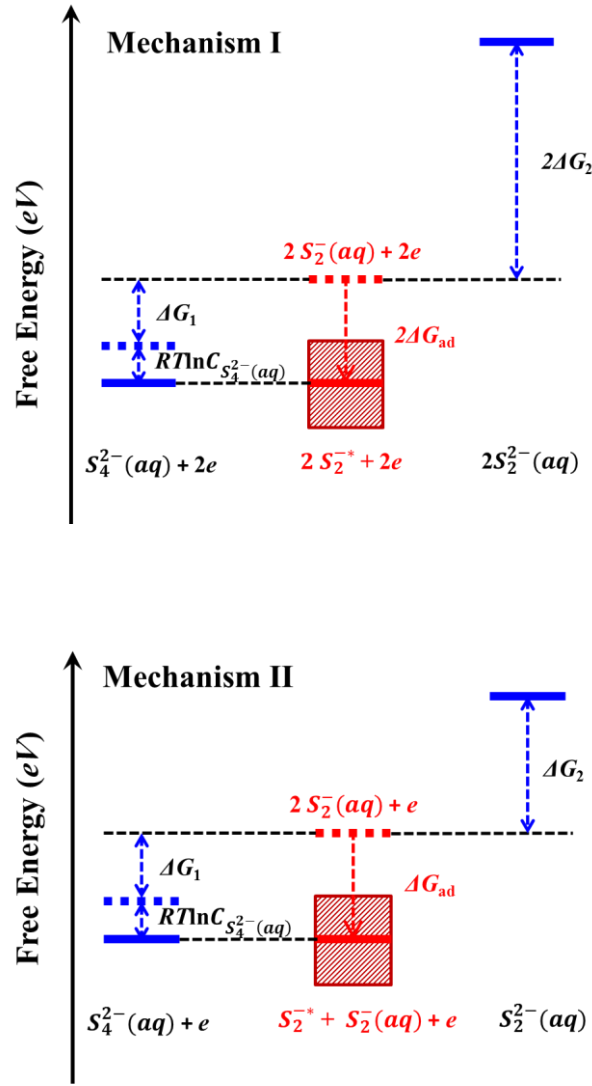
where $G_{S_2^-(aq)}$ and $G_{S_2^-*}$ are respectively the free energies of S_2^- in the aqueous solution and adsorbed at the water/electrode interface, which were obtained from the DFT total energies with the thermodynamic correction. The greater $G_{ad}^{S_2^-}$ is, the more strongly the species S_2^- binds to the electrode material.

Table S5. The Standard Gibbs Free Energy Variation of polysulphide dissociation

Reaction	ΔG (eV)
$S_4^{2-}(aq) \rightarrow S(aq) + S_3^{2-}(aq)$	2.50
$S_4^{2-}(aq) \rightarrow S^{2-}(aq) + S_3(aq)$	2.35
$S_4^{2-}(aq) \rightarrow S^{-}(aq) + S_3^{-}(aq)$	1.47
$S_4^{2-}(aq) \rightarrow S_2^{2-}(aq) + S_2(aq)$	1.10
$S_4^{2-}(aq) \rightarrow 2S_2^{-}(aq)$	0.20
$S_3^{2-}(aq) \rightarrow S^{2-}(aq) + S_2(aq)$	1.98
$S_3^{2-}(aq) \rightarrow S(aq) + S_2^{2-}(aq)$	2.76
$S_3^{2-}(aq) \rightarrow S^{-}(aq) + S_2^{-}(aq)$	1.36
$S_2^{2-}(aq) \rightarrow 2S^{-}(aq)$	2.28

Table S6. The standard reduction potentials E^{\ominus} v.s. RHE.

Reaction	E^{\ominus} (V) v.s. RHE
$S^{-}(aq) + e \rightarrow S^{2-}(aq)$	-0.31
$S_2^{-}(aq) + e \rightarrow S_2^{2-}(aq)$	-0.60
$S_3^{-}(aq) + e \rightarrow S_3^{2-}(aq)$	-0.24
$S_4^{-}(aq) + e \rightarrow S_4^{2-}(aq)$	-0.07
$S_4^{2-}(aq) + e \rightarrow S^{-}(aq) + S_3^{2-}(aq)$	-1.71
$S_4^{2-}(aq) + e \rightarrow S^{2-}(aq) + S_3^{-}(aq)$	-1.78
$S_4^{2-}(aq) + e \rightarrow S_2^{-}(aq) + S_2^{2-}(aq)$	-0.79
$S_3^{2-}(aq) + e \rightarrow S^{-}(aq) + S_2^{2-}(aq)$	-1.96
$S_3^{2-}(aq) + e \rightarrow S^{2-}(aq) + S_2^{-}(aq)$	-1.68
$S_2^{2-}(aq) + e \rightarrow S^{-}(aq) + S^{2-}(aq)$	-2.59
$S_4^{2-}(aq) + 2e \rightarrow S^{2-}(aq) + S_3^{2-}(aq)$	-2.02
$S_4^{2-}(aq) + 2e \rightarrow 2S_2^{2-}(aq)$	-1.39
$S_3^{2-}(aq) + 2e \rightarrow S^{2-}(aq) + S_2^{2-}(aq)$	-2.27
$S_2^{2-}(aq) + 2e \rightarrow 2S^{2-}(aq)$	-2.90



Scheme S1. The framework to evaluate the appropriate range of free adsorption energy of S_2^- ($G_{ad}^{S_2^-}$) over different electrode materials

Kinetically, the chemical potential always stepwise goes downhill for a sequential multi-elementary-step reaction occurred on the solid catalyst surface at the steady state,^{14,15} i.e. $\mu_{S_4^{2-}(aq)} + 2\mu_e \geq 2\mu_{S_2^*} + 2\mu_e \geq 2\mu_{S_2^-(aq)}$, where μ_e denotes the chemical potential of electron and $\mu_{S_2^*}$. Due to the slight endothermic process of $S_4^{2-}(aq) \rightarrow 2S_2^-(aq)$ ($\Delta G_1 = 0.20$ eV) and the negative E^\ominus for $S_2^-(aq) + e \rightarrow S_2^{2-}(aq)$ ($E^\ominus = -0.60$ V, $\Delta G_2 = 0.60$ eV), the reaction rate will reach the maxima when $\mu_{S_4^{2-}(aq)} + 2\mu_e = 2\mu_{S_2^*} + 2\mu_e = 2\mu_{S_2^-(aq)}$. Since $\mu_{S_2^*}$ is defined by Cheng *et al*¹² as follows:

$$\mu_{S_2^{-*}} = G_{S_2^{-*}}^o + RT \ln \frac{\theta_{S_2^{-*}}}{\theta_*}$$

where $\theta_{S_2^{-*}}$ and θ_* are respectively the coverages of adsorbed S_2^{-*} and free site $*$.

To screen the possible best catalyst, the optimal $RT \ln \frac{\theta_{S_2^{-*}}}{\theta_*}$ is better to be located in a small range of $[-\epsilon, \epsilon]$ where $\epsilon = 0.12$ eV at 298.15 K.¹⁵ Considering about the concentration of $S_4^{2-}(aq)$ about 0.25 mol/L¹⁶, as illustrated in Scheme S1, if following mechanism (I), the free adsorption energy of S_2^- ($G_{ad}^{S_2^-}$) for the optimal catalyst should be located in the range of:

$$\frac{1}{2}(\Delta G_1 - RT \ln C_{S_4^{2-}(aq)}) - \epsilon \leq G_{ad}^{S_2^-} \leq \frac{1}{2}(\Delta G_1 - RT \ln C_{S_4^{2-}(aq)}) + \epsilon$$

namely, $G_{ad}^{S_2^-} \in [0.00, 0.23]$ eV

If following mechanism (II), $G_{ad}^{S_2^-}$ should be located in the range of :

$$(\Delta G_1 - RT \ln C_{S_4^{2-}(aq)}) - \epsilon \leq G_{ad}^{S_2^-} \leq (\Delta G_1 - RT \ln C_{S_4^{2-}(aq)}) + \epsilon$$

namely, $G_{ad}^{S_2^-} \in [0.12, 0.35]$ eV

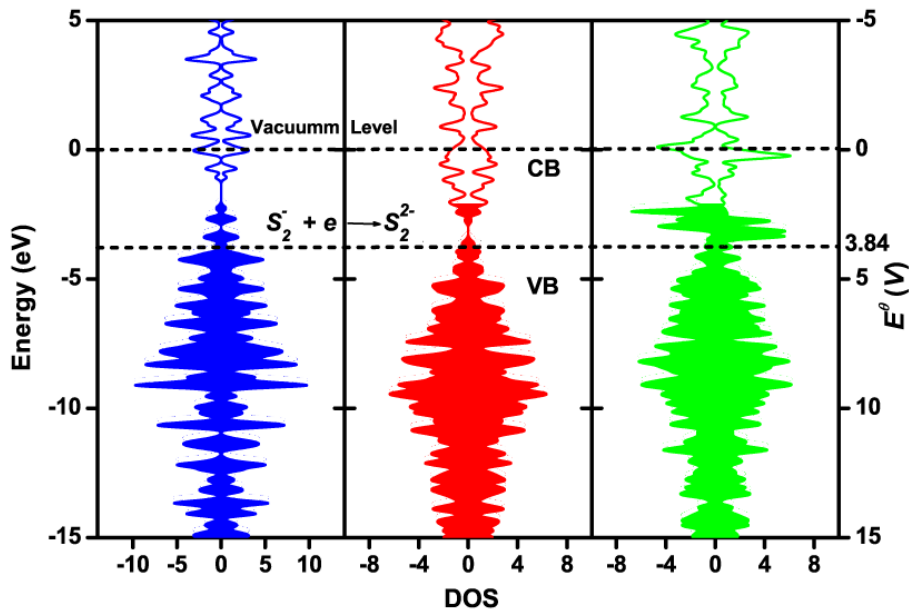


Fig. S9. The calculated density of states (DOS) of graphene (blue), N-graphene (red) and Co-N₄@graphene (green). The energy level and standard reduction potential of vacuum level and S_2^-/S_2^{2-} are shown in the Fig. as dash lines. The valence band (VB) and the conduction band (CB) of the electrode are respectively labeled via filled with color or without color.

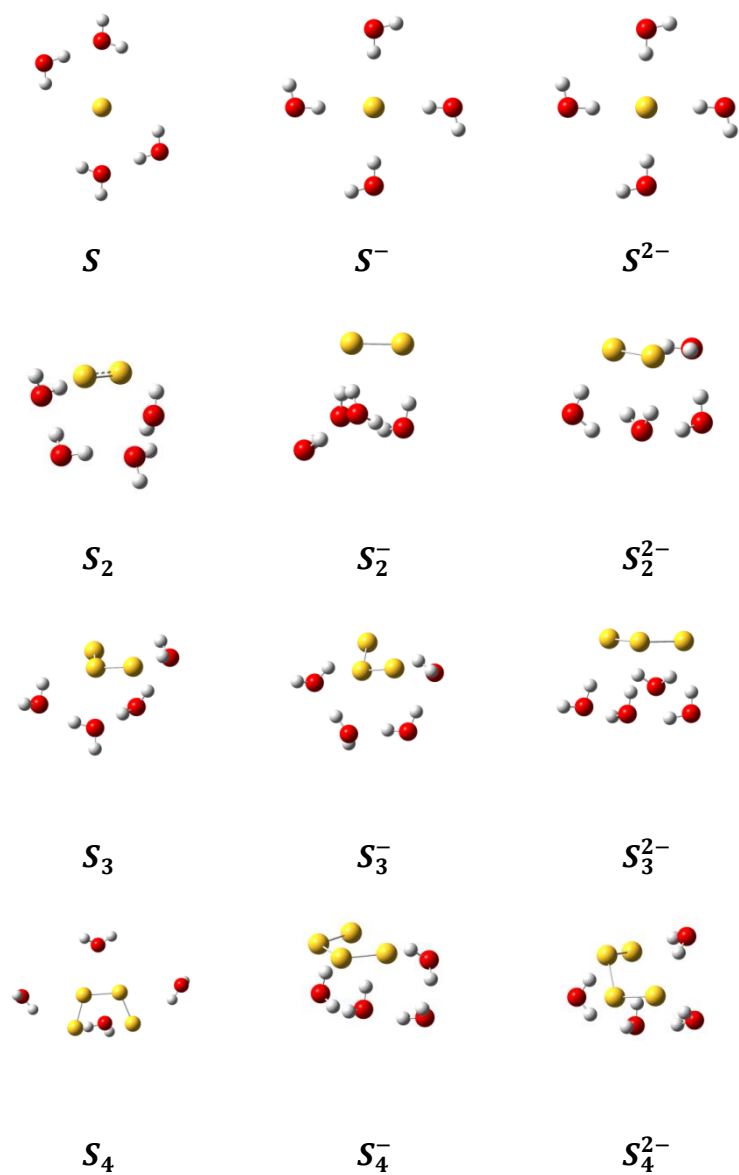


Fig. S10. The optimized geometry structure of neutral, monoanionic and dianionic $S_n(H_2O)_4$ cluster (n=1~4)

5 References

- 1 J. Du, Z. L. Du, J.-S. Hu, Z. X. Pan, Q. Shen, J. K. Sun, D. H. Long, H. Dong, L. T. Sun and X. H. Zhong, *J. Am. Chem. Soc.*, 2016, **138**, 4201–4209.
- 2 H. Zhang, K. Cheng, Y. M. Hou, Z. Fang, Z. X. Pan, W. J. Wu, J. L. Hua and X. H. Zhong, *Chem. Commun.*, 2012, **48**, 11235–11237.
- 3 H. C. Chen, F. G. Sun, J. T. Wang, W. C. Li, W. M. Qiao, L. C. Ling and D. H. Long, *J. Phys. Chem. C*, 2013, **117**, 8318–8328.
- 4 S. Jiao, J. Du, Z. L. Du, D. H. Long, W. Y. Jiang, Z. X. Pan, Y. Li and X. H. Zhong, *J. Phys. Chem. Lett.*, 2017, **8**, 559–564.
- 5 V. Barone and M. Cossi, *J. Phys. Chem. A*, 1998, **102**, 1995–2001.
- 6 S. Trasatti, *Pure & Appl. Chem.*, 1986, **58**, 955–966.
- 7 J. P. Perdew, K. Burke and Y. Wang, *Phys. Rev. B*, 1996, **54**, 16533–16539.
- 8 S. Grimme, S. Ehrlich and L. Goerigk, *J. Comput. Chem.*, 2011, **32**, 1456–1465.
- 9 G. Kresse and J. Furthmüller, *Phys. Rev. B: Condens. Matter.*, 1996, **54**, 11169–11186.
- 10 L. Yu, X. Pan, X.-M. Cao, P. Hu and X. H. Bao, *J. Catal.*, 2011, **282**, 183–190.
- 11 Y. Hou, D. Wang, X. H. Yang, W. Q. Fang, B. Zhang, H. F. Wang, G. Z. Lu, P. Hu, H. J. Zhao and H. G. Yang, *Nature Commun.*, 2017, **4**, 1583–1590.
- 12 J. Cheng, P. Hu, *Angew. Chem. Int. Ed.*, 2011, **50**, 7650–7654.
- 13 X. J. Cui, J. P. Xiao, Y. H. Wu, P. P. Du, R. Si, H. X. Yang, H. F. Tian, J. Q. Li, W.-H. Zhang, D. H. Deng and X. H. Bao, *Angew. Chem. Int. Ed.*, 2016, **55**, 6708–6712.
- 14 S. Licht, G. Hodes and J. Manassen, *Inorg. Chem.*, 1986, **25**, 2486–2489.
- 15 Y. Zhao and D. G. Truhlar, *Theor. Chem. Acc.*, 2008, **120**, 215–241.
- 16 F. Weigend and R. Ahlrichs, *Phys. Chem. Chem. Phys.*, 2005, **7**, 3297–3305.